

BCSJ Award Article

Face-to-Face Dimeric Tetrathiafulvalenes and Their Cation Radical and Dication Species as Models of Mixed Valence and π-Dimer States

Masashi Hasegawa,*[1] Kota Daigoku,[2] Kenro Hashimoto,[3] Hiroyuki Nishikawa,[4] and Masahiko Iyoda*[3]

[1]Department of Chemistry, School of Science, Kitasato University, 1-15-1 Kitasato, Minami-ku, Sagamihara, Kanagawa 252-0373

[2]Division of Chemistry, Center for Natural Sciences, College of Liberal Arts and Sciences, Kitasato University, 1-15-1 Kitasato, Minami-ku, Sagamihara, Kanagawa 252-0373

[3]Department of Chemistry, Graduate School of Science and Engineering, Tokyo Metropolitan University, Hachioji, Tokyo 192-0397

[4]Faculty of Science, Ibaraki University, 2-1-1 Bunkyo, Mito, Ibaraki 310-8512

Received July 25, 2011; E-mail: masasi.h@kitasato-u.ac.jp, iyoda@tmu.ac.jp

Intramolecular interactions of face-to-face tetrathiafulvalenes (TTFs) in 1,8-bis(tetrathiafulvalenyl)naphthalene frameworks were investigated in neutral and cationic states. From X-ray analysis and NMR spectroscopy on neutral 1,8-bis(tetrathiafulvalenyl)naphthalenes, which exist as a mixture of *syn*- and *anti*-isomers in solution, there is steric repulsion between TTF moieties. However, analysis of the cyclic voltammogram (CV) revealed that a strong attractive interaction was present in the cation radical state. Electronic spectra of the cation radical state showed the presence of a mixed-valence (MV) state with a strong charge resonance feature. ESR spectra of the 1,8-bis(tetrathiafulvalenyl)naphthalene cation radical showed a typical signal of an MV state. Furthermore, a π-dimer, which exhibits pronounced Davydov splitting in the electronic spectra, was formed in the dication state. The observed absorption bands in the electronic spectra were characterized by using quantum chemical calculations of the cation radical and dication species. NMR spectra of both the π-dimer and tetracation species show either a deshielding effect due to cationic charge or a shielding effect due to diamagnetic ring currents. To our knowledge, this is the first reported example of a ^{1}H NMR spectrum of TTF π-dimer.

Tetrathiafulvalene (TTF) and its derivatives can be easily oxidized to form stable cation radicals and dications, and these cationic species have been employed extensively in the development of new organic metals, superconductors, and semiconductor devices.[1,2] The ability of TTFs to readily self-aggregate in the cation radical state and form columnar structures, which act as conductive pathways in the solid state,[3] is of great interest from the viewpoint of a bottom-up approach to constructing supramolecular structures and nanoscale architectures.[3,4] Thus, a detailed understanding of the face-to-face interactions between TTFs is essential not only for elucidating the electronic state of organic metals but also for designing functionalized nanostructures based on TTF.

Face-to-face TTF dimers can be regarded as the simplest model for columnar stacks of TTFs. Typical stacking modes for face-to-face TTFs in neutral and/or cationic states are summarized in Scheme 1. In the solid state, neutral TTFs weakly stack to form dimers or columnar structures through S···S and π–π interactions (**A**), whereas neutral TTFs easily dissociate in solution.[1–3] In contrast, π-extended TTF derivatives and TTFs having amphiphilic properties self-associate even in solution, resulting in the formation of nanostructures.[5–7] Furthermore, stronger molecular interactions occur in mixed valence (MV) states with strong charge resonance (CR) (**B**). Electronic coupling in the MV state of dimeric $(TTF)_2^{\bullet+}$ shows Robin–Day Class II–III behavior on the basis of Müllken–Hush analysis of their intervalence charge-transfer (IV-CT) band.[8,9] Although paramagnetic $TTF^{\bullet+}$ exists as a monomer in solution at room temperature,[9a] diamagnetic π-dimer **C** is formed at lower temperatures in solution, except under certain conditions when supramolecular cages are formed.[10] As for **C**, Torrance et al. have reported a large blue shift in the electronic spectra, known as a Davydov blue shift.[11,12] In the case of TTF dications **D**, the two dications easily dissociate due to Coulombic repulsion.

A variety of TTF dimers and oligomers have been reported to form MV and π-dimer states.[3,12] However, there are some

Published on the web December 30, 2011; doi:10.1246/bcsj.20110224

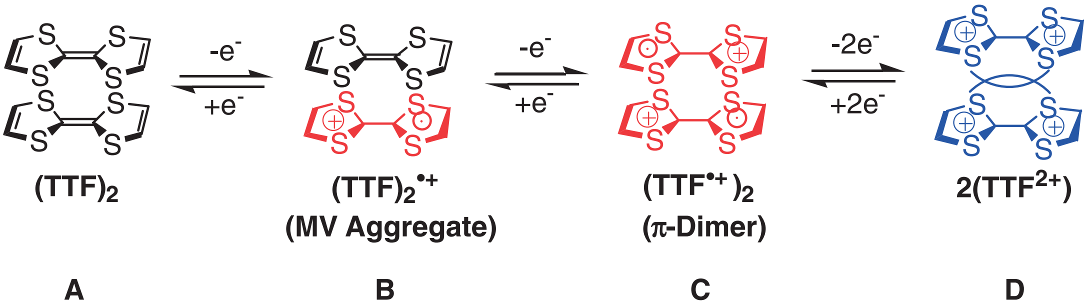

Scheme 1. Interactions between TTFs in a face-to-face manner.

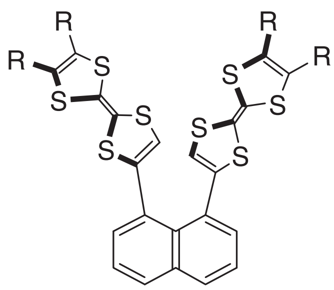

1a: R, R = SCH_2CH_2S
1b: R = SCH_3
1c: R = H

Chart 1.

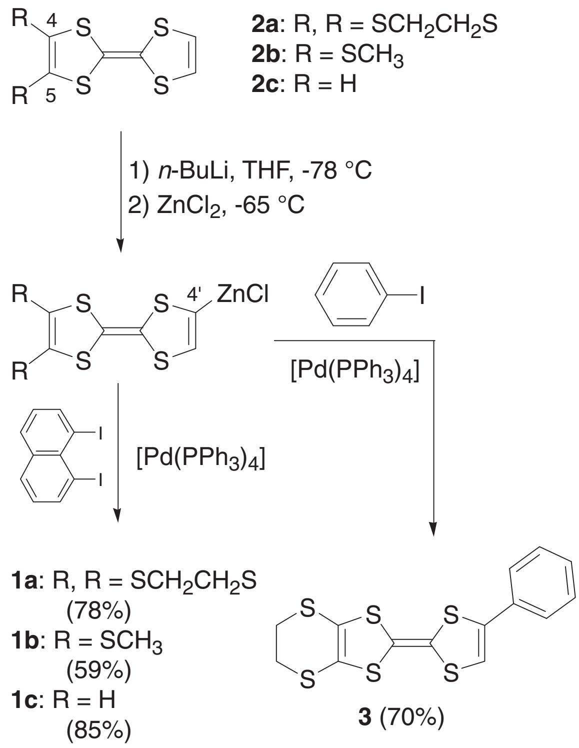

Scheme 2. Synthesis of **1a–1c** and **3**.

ambiguities in the reported MV and π-dimer states of TTFs in solution because the formation of those states are discussed on the basis of various spectroscopic data.[12c,13] In order to obtain accurate spectroscopic information about the MV and π-dimer states of TTFs, we prepared 1,8-bis(tetrathiafulvalenyl)naphthalenes **1a–1c** (Chart 1) as a model system. Since two TTF units are attached at the 1,8-positions of the naphthalene ring in **1a–1c**, the face-to-face interactions between two TTFs can be determined very easily.

We have previously reported the syntheses, structures, and properties of **1a–1c**.[14] In this paper, we focus on the face-to-face interactions between TTFs in the MV and π-dimer states, which can be utilized to construct supramolecular architectures. Furthermore, the electronic spectra of aggregated $(TTF)_2{}^{\bullet+}$ and $(TTF^{\bullet+})_2$ in the MV and π-dimer states, respectively, were corroborated via excitation energy calculations based on a time-dependent density functional theory (TD-DFT) method.

Results and Discussion

Synthesis. 1,8-Bis(tetrathiafulvalenyl)naphthalenes **1a–1c** were synthesized by using palladium-mediated coupling of organozinc intermediates,[12b,15] as shown in Scheme 2. For example, the reaction of bis(alkylthio)-TTFs **2a** and **2b** or TTF (**2c**) with *n*-BuLi in THF, followed by addition of anhydrous $ZnCl_2$ at −65 °C, yielded an organozinc species. The reaction of the zinc species with 1,8-diiodonaphthalene in the presence of $[Pd(PPh_3)_4]$ produced the corresponding coupling products **1a–1c** in 78%, 59%, and 85% yields, respectively. In a similar manner, the palladium-mediated reaction of the zinc complex of **2a** with iodobenzene afforded **3** in 70% yield.

Molecular Structures of Neutral 1,8-Bis(tetrathiafulvalenyl)naphthalenes 1a–1c. 1,8-Bis(tetrathiafulvalenyl)naphthalenes **1a–1c** showed temperature-dependent NMR spectra due to interconversion between the *syn-* and *anti*-isomers. The ^{1}H NMR spectrum of **1a** at 25 °C showed averaged signals due to fast interconversion between *syn-* and *anti*-isomers, which decoalesced at ca. −75 °C, and two sets of signals were observed at −90 °C in an *anti-*/*syn*-isomer ratio of 93:7.[16] The values of the equilibrium constant ($K_{syn\text{–}anti}$) and free energy difference (ΔE) between the *syn-* and *anti*-isomers are summarized in Table 1. Since the ΔE values are in the order **1c** < **1b** < **1a**, the steric hindrance of the substituent on the TTF moieties dominates the molecular conformations in the neutral state.

Recrystallization of **1a** from CH_2Cl_2 and *i*-Pr_2O at 4 °C gave single crystals large enough for X-ray crystallographic analysis (Figure 1). The molecule has crystallographic C_2 symmetry with a twofold axis passing through the C(1)–C(2) bond to form an *anti*-conformation. The mean deviations of C(1) and C(6) from the naphthalene plane were determined to be 0.051 and −0.043 Å, respectively, by using a least-squares method.

Table 1. Energy Difference between the *syn*- and the *anti*-Isomers[a)]

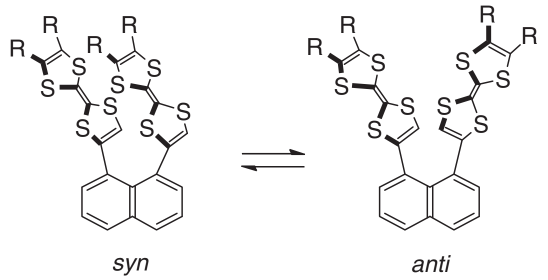

	Ratio[b)] (*syn*:*anti*)	$K_{syn\text{–}anti}$	$\Delta E_{syn\text{–}anti}$/kcal mol^{-1}
1a	7:93	13.3	0.94
1b	1:5	5.0	0.58
1c	2:7	3.5	0.45

a) In $CDCl_3$ solution at −90 °C. b) The ratios of the isomers were estimated from ^{1}H NMR signals of each TTF proton of **1a** and **1b** and that at the 2-position of naphthalene of **1c**, respectively.

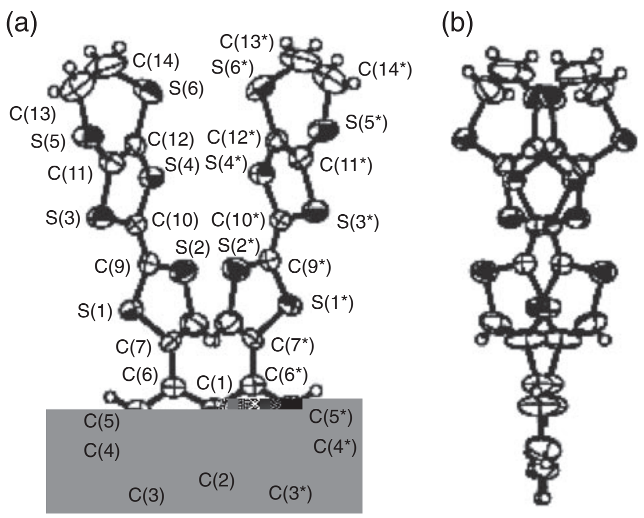

Figure 1. ORTEP drawing of **1a**: (a) top and (b) side views.

Thus, molecular strain is released by the *anti*-conformation of the TTF units and by the deformation of the naphthalene ring. The dihedral angle between the naphthalene and TTF rings was determined to be 54.6(3)°. The interatomic distances C(6)···C(6*) and C(7)···C(7*) were determined to be 2.50 and 2.76 Å, respectively, which are 3% and 8–9% shorter than those of previously reported 1,8-diarylnaphthalenes.[17] There are only two intermolecular S···S interactions within the sum of the van der Waals radii in the crystal.

Electrochemistry. In cyclic voltammograms of **1a**–**1c**, three reversible redox waves were observed, whereas in that of **3**, two reversible redox waves were observed (Figure 2 and Table 2). For **1a**–**1c**, the first and second waves were two one-electron processes, and the third wave was a two-electron process. Compound **3** shows oxidation potentials at −0.01 and 0.35 V under identical conditions. The first and second oxidation potentials of **1a** corresponding to the formation of $\mathbf{1a}^{\bullet+}$ and $\mathbf{1a}^{2+}$ are lower than the first potential of **3**, whereas the third oxidation

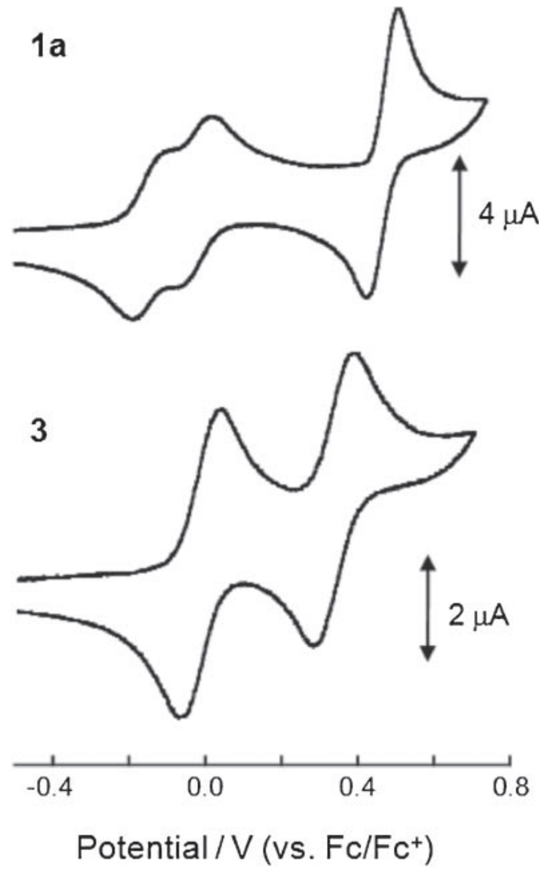

Figure 2. Cyclic voltammograms of **1a** and **3** in PhCN.

Table 2. Redox Potentials of **1a**–**1c**, **2a**–**2c**, and **3**[a)]

	$E^1_{1/2}$ /V	$E^2_{1/2}$ /V	$E^3_{1/2}$ /V	$E^2_{1/2} - E^1_{1/2}$ /V	K_c[b)]
1a	−0.18 (1e$^-$)	−0.05 (1e$^-$)	+0.44 (2e$^-$)	0.13	158
1b	−0.13 (1e$^-$)	−0.01 (1e$^-$)	+0.43 (2e$^-$)	0.12	107
1c	−0.23 (1e$^-$)	−0.13 (1e$^-$)	+0.42 (2e$^-$)	0.10	50
2a	0.01 (1e$^-$)		+0.35 (1e$^-$)	—	—
2b	−0.01 (1e$^-$)		0.32 (1e$^-$)	—	—
2c	−0.09 (1e$^-$)		0.28 (1e$^-$)	—	—
3	−0.01 (1e$^-$)		+0.35 (1e$^-$)	—	—

a) Conditions: in PhCN containing 0.1 M $n\text{-}Bu_4NClO_4$ at 25 °C; Ag/Ag^+ reference electrode, Pt counter and working electrodes, 100 mV s^{-1}; potentials referred to Fc/Fc^+. b) Comproportionation constant of the monocationic species: See Ref. 17.

potential of **1a** corresponding to the formation of the tetracation $\mathbf{1a}^{4+}$ is much higher than the second potential of **3**, owing to the face-to-face interactions in the mono-, di-, and tetracations of **1a**. The significant lowering of the first oxidation potential of **1a** compared with **3** is due to the formation of mixed-valence (MV) state as a result of charge delocalization between the two TTF moieties. The potential difference between the second oxidation of **1a** and the first oxidation of **3** may be attributed to the weakened conjugation between TTF and naphthalene moieties in **1a** compared with the conjugation between TTF and benzene moieties in **3**.[18] The higher third oxidation potential of **1a** than the second oxidation potential of **3** is due to the Coulombic interaction between the two TTF cation radicals.

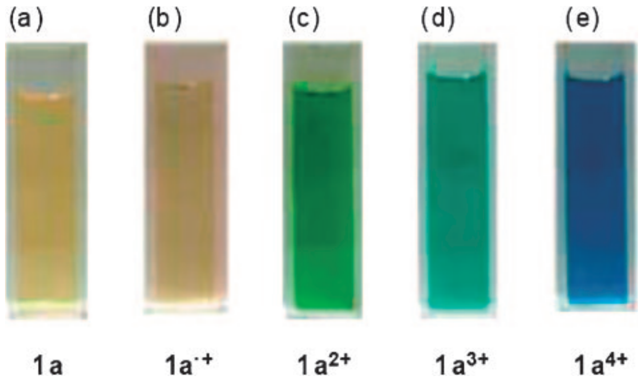

Figure 3. Color of (a) **1a**, (b) $\mathbf{1a^{\bullet+}}$, (c) $\mathbf{1a^{2+}}$, (d) $\mathbf{1a^{3+}}$, and (e) $\mathbf{1a^{4+}}$ in 1:1 CH_2Cl_2–MeCN.

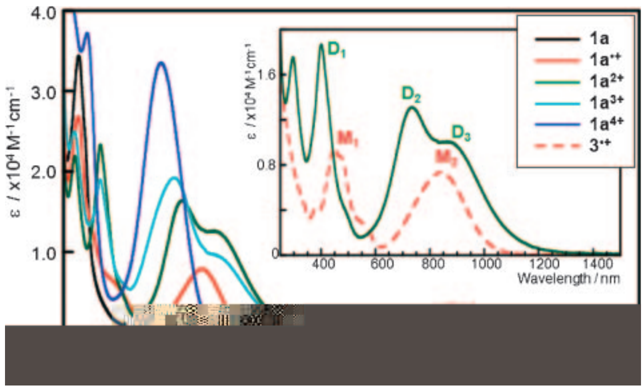

Figure 4. Electronic absorption spectra of **1a**, $\mathbf{1a^{\bullet+}}$, $\mathbf{1a^{2+}}$, $\mathbf{1a^{3+}}$, $\mathbf{1a^{4+}}$, and $\mathbf{3^{\bullet+}}$ in a 1:1 mixture of CH_2Cl_2–MeCN. The inset shows expanded electronic spectra of $\mathbf{1a^{2+}}$ together with $\mathbf{3^{\bullet+}}$ for comparison.

Table 3. Experimental and Calculated (TD B3LYP/6-31G(d)//HF/6-31G(d)) Longest Wavelength Absorption Maxima for **1a** and **3**, and Their Cation Radicals[a),b)]

	Experimental λ_{max}/nm (ε)	Calculated λ_{max}/nm (oscillator strength)
1a	312 (34000)	286 (0.334)
$\mathbf{1a^{\bullet+}}$ [c)]	312 (26000), 816 (7600), 1850 (3500)	315 (0.104), 862 (0.120), 1678 (0.056)
$\mathbf{1a^{2+}}$	402 (23000), 732 (18000), 858 (13000)	344 (0.202), 794 (0.204), 969 (0.177)
$\mathbf{1a^{3+}}$	400 (19000), 703 (19000), 860 (9700)	
$\mathbf{1a^{4+}}$	652 (30000)	673 (0.785)
3	314 (16000)	282 (0.169)
$\mathbf{3^{\bullet+}}$	448 (12000), 836 (9100)	372 (0.204), 852 (0.158)
$\mathbf{3^{\bullet+}}$ **(Solid)**[d)]	423, 715, 895	
$\mathbf{3^{2+}}$	644 (11000)	651 (0.219)

a) In a 1:1 mixture of CH_2Cl_2–MeCN. b) HF-optimized structures were used for the *anti*-isomer of **1** and $\mathbf{1^{4+}}$, and *syn*-isomer of $\mathbf{1^{2+}}$ in the TD-DFT calculations. c) The structure obtained from X-ray analysis[14b] was applied. d) The sample was cast on a quartz plate. See Supporting Information.

Similar redox behavior was observed in the cyclic voltammograms of **1b** and **1c**, although the first and second oxidation potentials were different. Relative thermodynamic stability of the cation radicals $\mathbf{1a^{\bullet+}}$, $\mathbf{1b^{\bullet+}}$, and $\mathbf{1c^{\bullet+}}$ was evaluated via the comproportionation constant K_c calculated from the difference between the first and second oxidation potentials.[19] The K_c values of **1a**, **1b**, and **1c** were determined to be 158, 107, and 50, respectively. The large values of K_c suggest the formation of a stable cation radical with strong interactions in the MV state, and the thioalkyl groups at the 4 and 5 positions stabilize the MV state compared to the unsubstituted MV state. Furthermore, coplanar ethylenedithio groups more effectively stabilize the MV state than two flexible methylthio groups.

Electronic Spectra. The electronic spectra of the cations of **1a–1c**, prepared by oxidation with $Fe(ClO_4)_3$, were acquired in 1:1 CH_2Cl_2–MeCN at room temperature.[20] Neutral **1a** showed the longest maximum absorption at 312 nm. The electronic spectra of **1b** and **1c** were similar, but oxidation of **1b** and **1c** with $Fe(ClO_4)_3$ produced unstable cation radicals. Therefore, we focused on the oxidation of **1a** for the investigation of the cationic states. Sequential addition of 1, 2, 3 equiv and excess amounts of $Fe(ClO_4)_3$ to 1:1 CH_2Cl_2–MeCN solutions of **1a** afforded five different colored solutions (Figure 3),[7e,21] i.e., electrochromism depending on the oxidation state.

Chemical titration of **1a** with 1 equiv of $Fe(ClO_4)_3$ gave $\mathbf{1a^{\bullet+}{\cdot}ClO_4^-}$. The electronic spectrum showed two absorption maxima at 312 and 816 nm, together with a broad absorption in the range of 1800–2200 nm (Figure 4). The absorption maximum at 816 nm was assigned to the intrinsic absorption of the TTF cation radical (SOMO$-$1 $\rightarrow$ SOMO),[22] and the broad absorption in the range of 1800–2200 nm was assigned to the CR band of $\mathbf{1a^{\bullet+}}$ due to the delocalization of the positive charge between the two TTF units in the MV state (Table 3). The CR band disappeared when $\mathbf{1a^{\bullet+}}$ was oxidized with a second equivalent of $Fe(ClO_4)_3$, and new absorption maxima were observed at 402, 732, and 860 nm. The face-to-face interactions between the two $TTF^{\bullet+}$ units result in the splitting of the longest absorption maximum around 750 nm. Thus, the absorption at 732 nm was assigned to an intrinsic transition of $TTF^{\bullet+}$ (D_2), and the absorption at 858 nm (D_3) was assigned to the HOMO–LUMO transition of π-dimer $\mathbf{1a^{2+}}$. Furthermore, the absorption maximum at 402 nm (D_1) was blue-shifted by 46 nm compared with that of $\mathbf{3^{\bullet+}}$ (M_1: $\lambda_{max} = 448$ nm). This pronounced blue shift is known as a Davydov blue shift and is due to the formation of a face-to-face π-dimer.[9–11] Interestingly, the electronic spectra of $\mathbf{3^{\bullet+}{\cdot}ClO_4^-}$ in the solid state showed the longest absorption maxima at 715 and 895 nm due to the formation of the π-dimer in the solid state (Figure S3c). Treatment of $\mathbf{1a^{2+}}$ with 1 equiv of $Fe(ClO_4)_3$ led to the

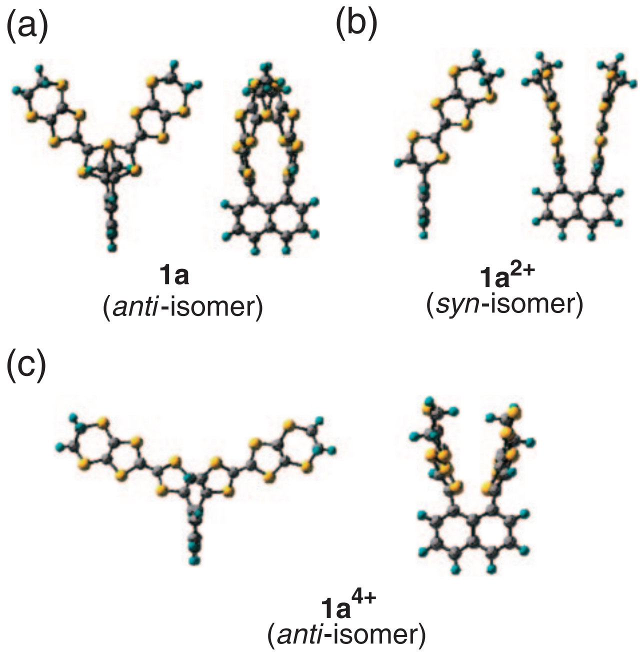

Figure 5. Optimized structures of **1a**, $\mathbf{1a^{2+}}$, and $\mathbf{1a^{4+}}$.

formation of $\mathbf{1a^{3+}}$, which showed absorption maxima at 400, 703, and 860 nm with a tail extending to 1600 nm. Addition of 1–3 equiv of $Fe(ClO_4)_3$ to $\mathbf{1a^{3+}}$ formed the tetracation $\mathbf{1a^{4+}}$, which showed the longest absorption maximum at 652 nm, similar to that of other TTF dications, such as $\mathbf{3^{4+}}$ ($\lambda_{max} =$ 644 nm).[22]

Theoretical Calculations. Geometry optimization was carried out at the RHF/6-31G(d) level for **1a**, $\mathbf{1a^{2+}}$, and $\mathbf{1a^{4+}}$, as well as **3** and its cation radicals.[23] For **1a**, two local minima, an *anti*-isomer with C_2 symmetry and a *syn*-isomer with C_1 symmetry, were found (Figure 5). Total energy of the former is lower than that of the latter by 3.4 kcal mol^{-1}, and the geometry of the *anti*-isomer is similar to that obtained from X-ray crystallographic analysis. In contrast, as for diamagnetic $\mathbf{1a^{2+}}$, the *syn*-isomer with C_s symmetry is more stable than the *anti*-isomer with C_2 symmetry by 3.2 kcal mol^{-1}. In *syn*-$\mathbf{1a^{2+}}$, the two TTF units are stacked in a face-to-face manner forming a stable π-dimer.[24] In tetracation $\mathbf{1a^{4+}}$, only the *anti*-isomer was an energy minimum. The two dithiolium cation rings in each TTF moiety were twisted by 21.6°, and the central C–C length of 1.447 Å is typical of those in the crystal structures of dicationic TTF species.[25]

To characterize the absorption bands, time-dependent (TD)-DFT calculations were performed at the B3LYP/6-31G(d) level. The geometries optimized by using the HF/6-31G(d) method were used,[26] except for paramagnetic $\mathbf{1a^{\bullet+}}$, for which the X-ray crystal structure (Figure 10a) was employed. Selected excitation energies and oscillator strengths are summarized in Table 3. For **1a**, the *anti*-conformation was chosen, and the calculation predicted an intense transition at 4.33 eV (286 nm), which corresponds to the lowest absorption band at 312 nm in the electronic spectra. Since the excitation to the π^*-type LUMO extending onto the naphthalene moiety is mixed in the wave function of the final state, the transition includes a contribution from intramolecular charge transfer.[27]

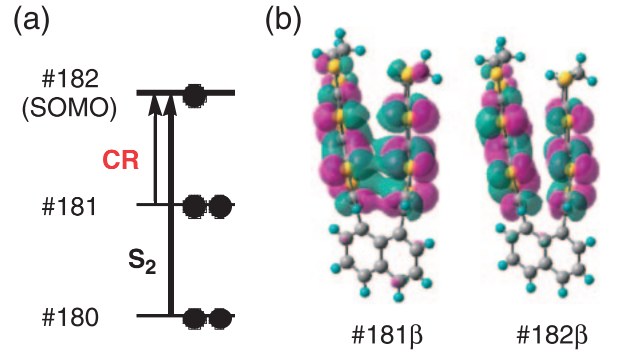

Figure 6. (a) Illustration of electronic transition of $\mathbf{1a^{\bullet+}}$. (b) MO of $\mathbf{1a^{\bullet+}}$. The wave function value of the MO surface is 0.02 bohr$^{-3/2}$.

In the case of $\mathbf{1a^{\bullet+}}$, the transition to the first excited state was calculated to be at 0.74 eV (1678 nm) and corresponds to the observed CR band (1850 nm), which involves a one-electron excitation from SOMO−1 (#181β) to the lowest vacant orbital (#182β). As seen in Figure 6b, these two MOs can be viewed as in-phase and out-of-phase combinations of the π orbitals of the TTF moieties, respectively. The absorption at 816 nm was attributed to the second excited state calculated at 1.44 eV (862 nm, S_2 in Figure 6a).[27]

Transitions in $\mathbf{3^{\bullet+}}$ and $\mathbf{1a^{2+}}$ and related MOs are illustrated in Figure 7. For the *syn*-isomer of $\mathbf{1a^{2+}}$, three states were obtained at 1.28 (969 nm), 1.56 (794 nm), and 3.61 eV (344 nm), to which the observed D_3, D_2, and D_1 bands were assigned, respectively (inset of Figure 4). D_3, which is the lowest in energy, is a HOMO–LUMO transition. The HOMO and LUMO involve in-phase and out-of-phase mixing of the SOMO in $\mathbf{3^{\bullet+}}$ (#95α and #95β in Figure 7), which is the TTF π-orbital. The D_2 band corresponds to the electronic transition from HOMO−2 (#179) to the LUMO in $\mathbf{1a^{2+}}$. HOMO−2 involves negative overlap of SOMO−1 (#94β) in $\mathbf{3^{\bullet+}}$, which is comprised of low-energy π-orbitals on the TTF moieties, whereas HOMO−1 (#180), which involves the naphthalene moiety, is not related to the D_2 transition.[27] In addition, calculations qualitatively reproduced the observed Davydov blue shift. The energy of D_2 is higher than that of the M_2 transition from SOMO−1 (#94β) to the SOMO (#94β) in $\mathbf{3^{\bullet+}}$. Similarly, the transition energy of D_1 (3.61 eV) is greater than that of M_1 in $\mathbf{3^{\bullet+}}$ (3.34 eV). Although D_1 involves a transition from the HOMO to LUMO+3 (#185) in $\mathbf{1a^{2+}}$, M_1 involves a transition from the SOMO (#95α) to LUMO+1 (#97α). LUMO+3 (#185) and LUMO+1 (#183) in $\mathbf{1a^{2+}}$ are the out-of-phase and in-phase combinations of LUMO+1 (#97α) in $\mathbf{3^{\bullet+}}$, respectively, supporting the Davydov blue shift observed in the electronic spectra.[27] LUMO+2 (#184), formed from orbital #98β in $\mathbf{3^{\bullet+}}$, is not involved in the D_1 transition.

Finally, a band at 1.84 eV (673 nm) was predicted for $\mathbf{1a^{4+}}$. The transitions from HOMO−2 (#178) to the LUMO (#181) and from HOMO−1 (#179) to LUMO+2 (#182) are responsible for this band. All four orbitals are located on the TTF^{2+} moieties.[27]

ESR and NMR Spectra of $\mathbf{1a^{\bullet+}\cdot ClO_4^-}$ and $\mathbf{3^{\bullet+}\cdot ClO_4^-}$. ESR spectra of paramagnetic $\mathbf{1a^{\bullet+}\cdot ClO_4^-}$ and $\mathbf{3^{\bullet+}\cdot ClO_4^-}$ in CH_2Cl_2–MeCN (1:1) are shown in Figure 8. The spectrum of $\mathbf{1a^{\bullet+}}$ showed hyperfine splitting with a binominal intensity ratio

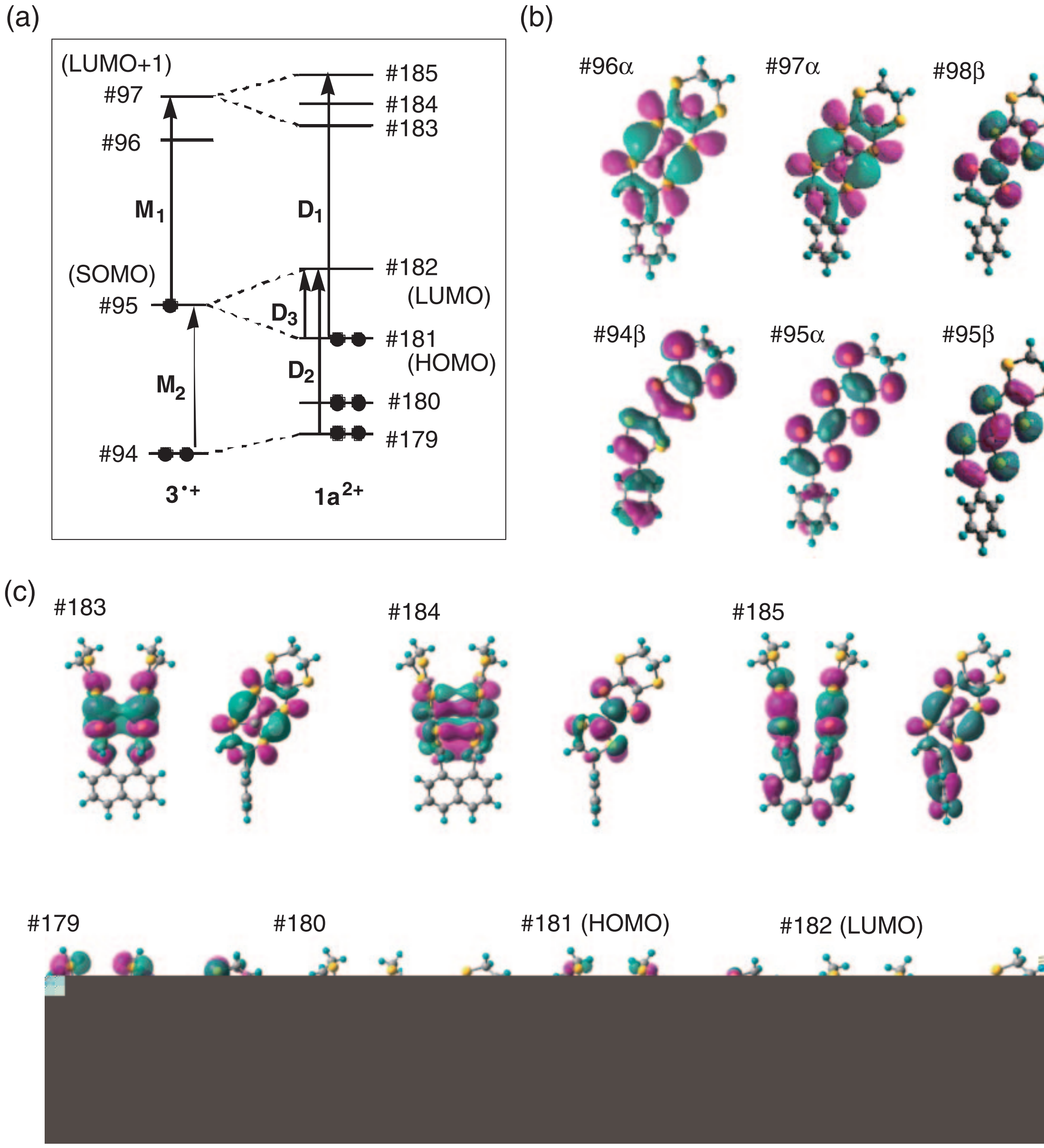

Figure 7. (a) Illustration of electronic transitions in $\mathbf{3}^{\bullet+}$ and $\mathbf{1a}^{2+}$ and MOs of (b) $\mathbf{3}^{\bullet+}$ and (c) $\mathbf{1a}^{2+}$. The wave function value of the MO surface is 0.02 bohr$^{-3/2}$.

of 1:2:1 at $g = 2.0066$. The two essentially equivalent protons of the EDT-TTF moieties in $\mathbf{1a}^{\bullet+}$ cause the hyperfine splitting, and the hyperfine coupling constant (hfcc) was 0.063 mT, which is almost half the value for the TTF monocation radical. The spectrum of $\mathbf{3}^{\bullet+}$ showed only hyperfine splitting with an intensity ratio of 1:1 (hfcc = 0.125 mT). Since both cation radicals showed almost 100 mol % unpaired spin content in the solution ESR spectra,[28] the half value of hfcc in $\mathbf{1a}^{\bullet+}$ compared with that of **3** is due to the stable MV state. In contrast to $\mathbf{1a}^{\bullet+}$, π-dimer $\mathbf{1a}^{2+}$ showed no ESR signal because it is diamagnetic.

As shown in Figure 9, ^{1}H NMR spectra for $\mathbf{1a}^{2+}$, $\mathbf{1a}^{4+}$, and $\mathbf{3}^{2+}$ in MeCN-d_3 were obtained. The TTF proton of $\mathbf{1a}^{2+}$ showed a broad peak at δ 7.45, showing the effect of the positive charge on the 1,3-dithiolium ion (**1a**: δ 6.03 for the TTF proton). A similar downfield shift was observed for the peak corresponding to the neighboring β proton of naphthalene ($\mathbf{1a}^{2+}$: δ 8.25; **1a**: δ 7.85). To the best of our knowledge, this is the first report of an NMR spectrum of a TTF π-dimer. Furthermore, the TTF proton of $\mathbf{1a}^{4+}$ (δ 8.94) was observed at a lower field than that of $\mathbf{1a}^{2+}$ owing to the higher positive charge on the molecules. However, in comparison with that of $\mathbf{3}^{2+}$ (δ 9.40), which shows a typical chemical shift for TTF dications,[25] the TTF proton of $\mathbf{1a}^{4+}$ was shifted upfield by 0.46 ppm, reflecting the shielding effect from the face-to-face aromatic 1,3-dithiolium cations. The neighboring β proton of naphthalene (δ 8.50) in $\mathbf{1a}^{4+}$ is deshielded due to the aromatic 1,3-dithiolium cations.

Solid-State Structure of $(\mathbf{1a})_2\cdot(\mathrm{I}_3)_{0.5}\cdot\mathrm{I}^{\bullet-}(\mathrm{I}_2)_{0.5}\cdot\mathrm{C}_6\mathrm{H}_5\mathrm{Cl}$ (4). Cationic species **4** was prepared by controlled electrolysis of **1a** at a constant potential in chlorobenzene in the presence of n-Bu_4NI_3 and was characterized by X-ray analysis. As shown in Figure 10a, the crystal lattice contains two different cation

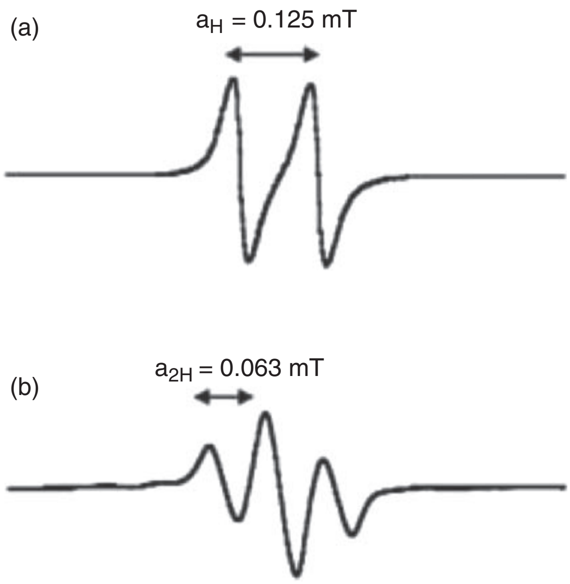

Figure 8. ESR spectra of (a) $\mathbf{3^{\bullet+}}$ (5.0×10^{-5} M) and (b) $\mathbf{1a^{\bullet+}}$ (1.3×10^{-4} M) in MeCN–CH_2Cl_2 at rt.

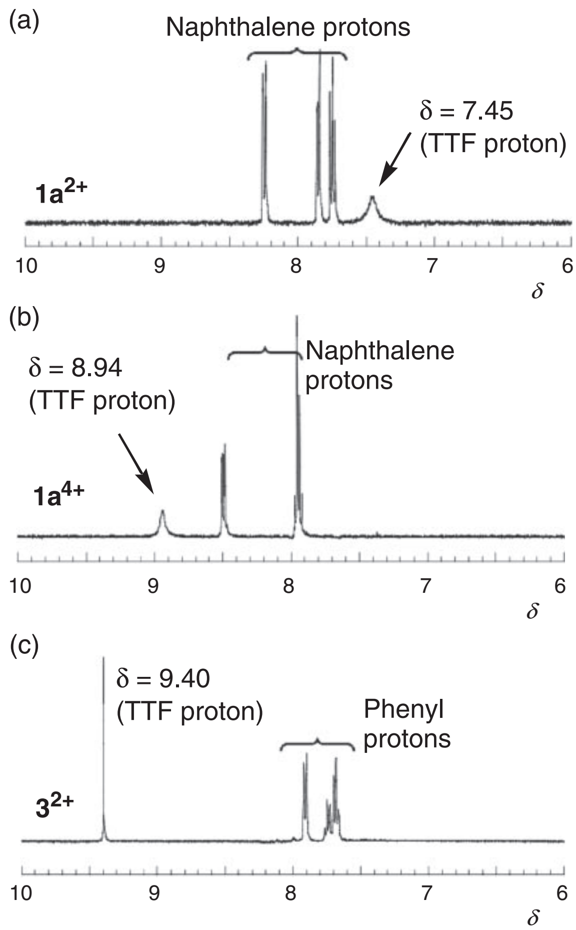

Figure 9. ^{1}H NMR spectra of (a) $\mathbf{1a^{2+}}$, (b) $\mathbf{1a^{4+}}$, and (c) $\mathbf{3^{2+}}$.

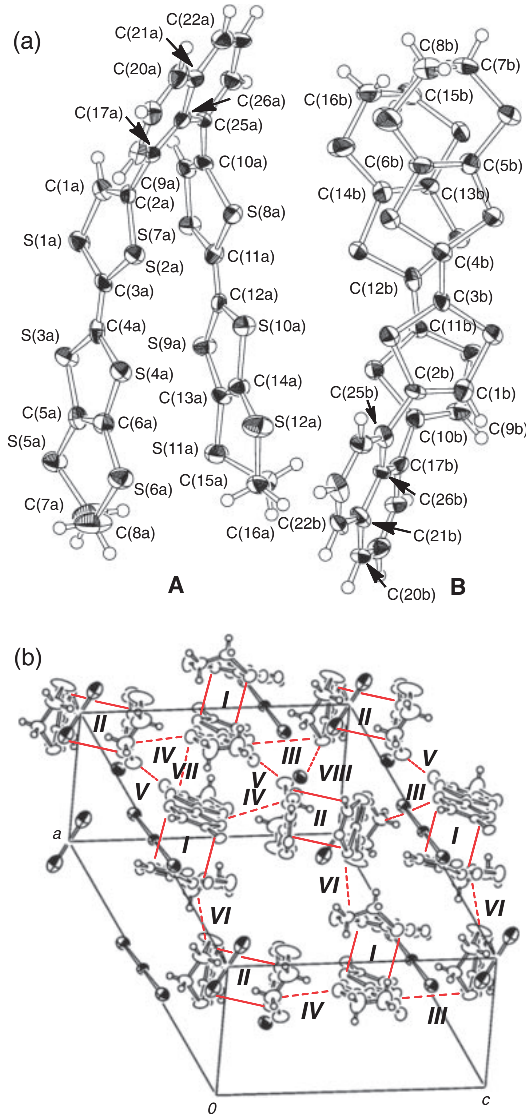

Figure 10. ORTEP diagram of $(\mathbf{1a})_2 \cdot (I_3)_{0.5} \cdot I^{\bullet-}(I_2)_{0.5} \cdot C_6H_5Cl$. (a) Molecular structure of **4**. **A** and **B** are two crystallographically independent molecules. Selected bond lengths [Å] and angles [°]: C(1a)–C(2a) 1.36(1), C(3a)–C(4a) 1.35(1), C(5a)–C(6a) 1.35(1), C(11a)–C(12a) 1.36(1), C(1b)–C(2b) 1.36(1), C(3b)–C(4b) 1.35(1), C(5b)–C(6b) 1.38(1), C(11b)–C(12b) 1.37(1), C(17a)–C(26a)–C(25a) 127.3, C(20a)–C(21a)–C(22a) 118.6, C(17b)–C(26b)–C(25b) 125.8, C(20b)–C(21b)–C(22b) 119.8. (b) Packing diagram. Chlorobenzene and naphthalene ring carbons except for C(17a) and C(25a) are omitted for clarity. The solid lines indicate the intramolecular interaction of two TTF units, the dashed lines corresponding to the intermolecular interaction of two TTF units (short contacts [Å], *I* in **A**: S(1a)⋯S(7a) 3.69 and S(2a)⋯S(8a) 3.46 Å; *II* in **B**: S(1b)⋯S(7b) 3.70 and S(2b)⋯S(8b) 3.51; *III*: S(7a)⋯S(8b) 3.39 and S(7a)⋯S(10b) 3.70; *IV*: S(2b)⋯S(12a) 3.67; *V*: S(1a)⋯S(5b) 3.66, S(1b)⋯S(3a) 3.56, and S(1b)⋯S(5a) 3.66; *VI*: S(8a)⋯S(12b) 3.56, S(8a)⋯S(10b) 3.58, and S(12a)⋯S(8b) 3.69; *VII*: S(3a)⋯S(4a) 3.60; *VIII*: S(3b)⋯S(7b) 3.64 and S(5b)⋯S(7b) 3.53.

radicals, I_3^-, I_2, I^-, and chlorobenzene. Taking into account that the ratio of the molecules of **1a** and the anionic charges based on I_3^- and I^- is 4:3, cation radical **4** possesses an average charge per molecule of **1a** of +0.75. The two cation radicals (**1a$_2$$^{1.5+}$**) adopt a *syn*-conformation (Figure 10a), reflecting the stability of the face-to-face stacking structure in the cation radical and dication states. Interestingly, these dimeric TTFs are aligned in an edge-to-face mode to form a two-dimensional sheet structure (Figure 10b). The dihedral angles between the naphthalene and TTF rings were determined to be 52°–56°. Although one TTF ring adopts a planar structure with a maximum deviation of 0.1 Å from the least-squares plane, the other three TTF rings have bent 1,3-dithiole rings. The *syn* arrangement of the TTF moieties causes the 1,3-dithiole rings to form envelope-like structures, and the intramolecular distances between S(1a)···(7a), S(2a)···(8a), S(1b)···(7b), and S(2b)···(8b) are shorter than the sum of the van der Waals radii (3.70 Å). Although there is only one short S···I contact in **4** (I_2···S(9b) 3.53 Å), there are a number of short intermolecular S···S contacts, as shown in Figure 10b, and these S···S contacts result in the formation of a sheet structure. In spite of the κ-like structure,[29] electric conductivity of **4** was not very high (5.0×10^{-5} S cm^{-1}), which is thought to be due to inhibition of the *b* axis conductivity pathway by the naphthalene moiety. Moreover, **4** in DMSO underwent a charge recombination, and in the UV–vis–NIR spectrum of **4** in DMSO, absorptions at 836 (SOMO−1 → SOMO) and 1800 nm (CR band) were observed, similar to those in the spectrum of **1a**$^{\bullet+}$ shown in Figure 4.[27] Finally, X-ray analysis of **4** experimentally confirmed that the *syn*-conformation in the cation radical and dication states of **1a** was much more stable than the corresponding *anti*-conformation, although neutral **1a** existed as a mixture of two isomers in solution in an *anti*–*syn* ratio of 93:7 (Table 1) and adopted the *anti*-form in the solid state (Figure 1) in order to avoid steric crowding.

Conclusion

We studied in detail the interactions between two TTF units by using 1,8-bis(tetrathiafulvalenyl)naphthalenes **1a**–**1c** as a model. From X-ray analyses and molecular structural calculations, the *anti*-isomer of neutral **1a**–**1c** is more stable than the *syn*-isomer due to steric effect, although **1a**–**1c** exist as a mixture of *anti*- and *syn*-isomers in solution. CV measurements revealed that **1a**–**1c** underwent two one-electron and one two-electron redox processes. Large K_c values were obtained due to a stable mixed-valence (MV) state in **1a**–**1c**, and the thioalkyl groups at the 4 and 5 positions of the TTF moieties stabilize the MV state. Cationic species **1a**$^{\bullet+}$, **1a**$^{2+}$, and **1a**$^{4+}$ were prepared by chemical and electrochemical oxidation methods, and their electronic structures were elucidated from absorption spectra. In the case of **1a**$^{\bullet+}$, a strong charge resonance (CR) band was observed arising from the MV state due to the face-to-face arrangement of the TTF moieties. For **1a**$^{2+}$, the lowest energy absorption band was split, indicating a Davydov blue shift due to the formation of a π-dimer. The experimentally observed transitions could be reproduced by TD-DFT calculations. From an ESR spectrum of **1a**$^{\bullet+}$, a hyperfine coupling constant (hfcc) consistent with that for an MV state was obtained. The ^{1}H NMR spectra of **1a**$^{2+}$ and **1a**$^{4+}$ were consistent with the formation of stable π-dimers. To the best of our knowledge, this is the first report of NMR spectra of a diamagnetic TTF π-dimer. Our results provide detailed information about the interactions in the MV and π-dimer states of TTF derivatives and will be useful in the design of supramolecular structures and functional nanostructures.

Experimental

1,8-Bis[(4,5-ethylenedithio)tetrathiafulvalenyl]naphthalene (1a). To a solution of **2a** (770 mg, 2.6 mmol) in THF (40 mL) was added *n*-C_4H_9Li (1.65 mL, 2.6 mmol) dropwise at −78 °C under N_2 atmosphere. The mixture was stirred for 90 min. Then, a suspension of anhydrous $ZnCl_2$ (442 mg, 3.2 mmol) in THF (3 mL) was added to the reaction mixture at −65 °C. The mixture was stirred for 1 h at the same temperature and warmed up to −20 °C. A solution of 1,8-diiodonaphthalene (355 mg, 0.9 mmol) in THF (2 mL) and [$Pd(PPh_3)_4$] (216 mg, 0.19 mmol) was added. The mixture was stirred for 1 h at −20 °C and warmed up to 45 °C. After stirring for 18 h, aqueous NH_4Cl solution was added to the mixture and extracted with CS_2. The combined organic layer was washed with saturated brine and dried over $MgSO_4$. The solution was filtered, and solvent was removed in vacuo. The residue was purified by column chromatography on silica gel (activity V) with CS_2 as the eluent. Recrystallization from CS_2–diisopropyl ether gave red crystals of **1a** (513 mg, 78%). **1a**: mp 199.3–200.4 °C; LDI-TOF-MS $m/z = 712$ (M^+); ^{1}H NMR ($CDCl_3$:CS_2 = 1:1, 500 MHz): δ 7.85 (dd, $J = 7.5$ and 1.2 Hz, 2H), 7.56 (dd, $J = 7.5$ and 1.2 Hz, 2H), 7.46 (t, $J = 7.5$ Hz, 2H), 6.03 (s, 2H), 3.29 (s, 8H); ^{13}C NMR ($CDCl_3$:CS_2 = 1:1, 125 MHz): δ 135.2, 133.2, 131.0, 130.4, 129.5, 125.4, 118.4, 114.8, 114.2 (2C), 105.4 (2C), 30.5; UV–vis–NIR (4.2×10^{-5} M, CH_2Cl_2): λ_{max} (ε) 312 (30000), 338sh (22000) nm; IR (KBr): 2957, 2923, 2853 cm^{-1}; Anal. Calcd for $C_{26}H_{16}S_{12}$: C, 43.79; H, 2.26%. Found: C, 43.63; H, 2.25%.

1,8-Bis[4,5-bis(methylthio)tetrathiafulvalenyl]naphthalene (1b). The synthesis of **1b** was carried out from **2b** and 1,8-diiodonaphthalene in 59% yield in a similar manner as described for **1a**. **1b**: a red powder; mp 86.9–87.8 °C; MALDI-TOF-MS $m/z = 716$ (M^+); ^{1}H NMR ($CDCl_3$, 500 MHz): δ 7.88 (dd, $J = 7.5$ and 1.2 Hz, 2H), 7.58 (dd, $J = 7.5$ and 1.2 Hz, 2H), 7.48 (t, $J = 7.5$ Hz, 2H), 6.07 (s, 2H), 2.47 (s, 6H), 2.44 (s, 6H); ^{13}C NMR ($CDCl_3$, 125 MHz): δ 135.1, 133.5, 130.9, 130.3, 129.4, 127.9, 126.7, 125.4, 117.8, 115.4, 106.8 (2C), 19.3 (2C); UV–vis–NIR (2.5×10^{-5} M, CH_2Cl_2): λ_{max} (ε) 308 (33000), 390sh (5800) nm; IR (KBr): 2918, 2853 cm^{-1}; Anal. Calcd for $C_{26}H_{20}S_{12}$: C, 43.54; H, 2.81%. Found: C, 43.34; H, 3.05%.

1,8-Bis(tetrathiafulvalenyl)naphthalene (1c). The synthesis of **1c** was carried out from tetrathiafulvalene and 1,8-diiodonaphthalene in 85% yield in a similar manner as described for **1a**. **1c**: an orange powder; mp 145.6–146.7 °C; LDI-TOF-MS $m/z = 532$ (M^+); ^{1}H NMR ($CDCl_3$, 400 MHz): δ 7.86 (dd, $J = 8.0$ and 1.0 Hz, 2H), 7.60 (dd, $J = 8.0$ and 1.0 Hz, 2H), 7.46 (t, $J = 8.0$ Hz, 2H), 6.30 (d, $J = 6.8$ Hz, 2H), 6.28 (d, $J = 6.8$ Hz, 2H), 6.05 (s, 2H); ^{13}C NMR ($CDCl_3$, 100 MHz): δ 135.2, 133.5, 130.9, 130.3, 129.8, 125.5, 119.2 (2C), 118.9, 118.1, 111.1, 110.7; UV–vis–NIR (4.2×10^{-5} M, CH_2Cl_2): λ_{max} (ε) 310 (30000), 400 (3100) nm; IR (KBr):

3061, 2924, 2853 cm^{-1}; Anal. Calcd for $C_{22}H_{12}S_8$: C, 49.59; H, 2.27%. Found: C, 49.31; H, 2.47%.

4,5-Ethylenedithio-4′-phenyltetrathiafulvalene (3). **3** was synthesized from **2c** and iodobenzene in 70% yield in a similar procedure as described for **1a**. **3**: an orange powder; mp 125.4–126.3 °C; MALDI-TOF-MS: $m/z = 370$ (M^+); ^{1}H NMR ($CDCl_3$, 500 MHz): δ 7.37 (d, $J = 8.3$ Hz, 2H), 7.34 (t, $J = 8.3$ Hz, 2H), 7.29 (t, $J = 8.3$ Hz, 1H), 6.48 (s, 1H), 3.28 (s, 4H); ^{13}C NMR ($CDCl_3$, 125 MHz): δ 136.0, 132.3, 128.9, 128.6, 126.3, 117.6, 114.0 (2C), 113.1, 105.4, 30.2 (2C); IR (KBr): 3063, 2957, 2923, 2852 cm^{-1}; UV–vis–NIR (7.1×10^{-5} M, CH_2Cl_2): λ_{max} (ε) 301sh (16500), 313 (16900), 336 (14264), 388sh (4150) nm; Anal. Calcd for $C_{14}H_{10}S_6$: C, 45.37; H, 2.72%. Found: C, 45.18; H, 2.74%.

X-ray Crystallographic Study. X-ray crystallographic measurements were made by using graphite-monochromated Mo Kα ($\lambda = 0.71069$ Å) radiation. The intensity data were collected with a Rigaku AFC-7R four-circle diffractometer at rt for **1a** and with a Rigaku RAXIS-RAPID Imaging Plate diffractometer at −80 °C. The structures were solved by direct method (SIR 92[30]) and refined by full-matrix least-squares methods. All non-hydrogen atoms were refined anisotropically, and hydrogen atoms were refined isotropically. Crystal data for **1a**: $C_{26}H_{16}S_{12}$, MW: 713.18, space group $C2/c$ (# 15), $a = 17.712(7)$ Å, $b = 16.313(3)$ Å, $c = 11.963(3)$ Å, $\beta = 121.78(2)°$, $V = 2938(1)$ Å^3, $Z = 4$, $D_{calcd} = 1.612$ g cm^{-3}, $R_1 = 0.048$, $R_w = 0.068$, GOF = 1.25. Among a total of 3602 reflections measured, 3372 were unique and the observed ($I > 2.00\sigma(I)$) 1242 reflections were used for the refinement. Crystal data for **4**: $2(C_{26}H_{16}S_{12})\cdot(C_6H_5Cl)\cdot(I_3^-)\cdot(I^-)\cdot(I_2)$, MW: 1982.99, space group $P\bar{1}$ (# 2), $a = 15.5971(1)$ Å, $b = 17.858(1)$ Å, $c = 14.3447(7)$ Å, $\alpha = 95.272(1)°$, $\beta = 116.992(2)°$, $\gamma = 75.435(1)°$, $V = 3444.7(3)$ Å^3, $Z = 2$, $D_{calcd} = 1.912$ g cm^{-3}, $R_1 = 0.065$, $R_w = 0.188$, GOF = 1.04. Among a total of 21099 reflections measured, 13435 were unique and the observed ($I > 2.00\sigma(I)$) 7599 reflections were used for the refinement. CCDC-181689 (**1a**) and CCDC-181690 (**4**) contain the supplementary crystallographic data. These data can be obtained free of charge from The Cambridge Crystallographic Data Centre via www.ccdc.cam.ac.uk/data_request/cif.

Chemical Oxidation Procedure. The chemical oxidation of **1a–1c** and **3** were performed with $Fe(ClO_4)_3$ as the oxidant in CH_2Cl_2–MeCN (v/v = 1:1) solution. The oxidant was titrated before use by aqueous EDTA–2Na solution and potassium thiocarbonate (KSCN) as the indicator. Chemical oxidation was carried out by addition of 0.1–6.0 equiv of $Fe(ClO_4)_3$ solution in MeCN–CH_2Cl_2 to the solution of either **1a** or **3**. After stirring for 2 min, the electronic spectra and the ESR spectra were recorded. ^{1}H NMR spectra were recorded after the replacement of the solvent to MeCN-d_3.

Theoretical Calculations. Geometry optimization was performed at the HF/6-31G(d) level for **1a**, **1a^{2+}**, **1a^{4+}**, **3**, and **3^{2+}** as well as UHF/6-31G(d) for **3$^{\bullet+}$**. For **1a**, **1a^{2+}**, and **1a^{4+}**, both *syn-* and *anti*-conformations were elucidated. All optimized geometries were confirmed to be at potential minima by harmonic vibrational analysis. Time-dependent (TD) DFT calculations were carried out at the B3LYP/6-31G(d) level. For **1a$^{\bullet+}$**, the geometry obtained from X-ray crystallographic analysis **4** was used.

This work was partly supported by a Grant-in-Aid for Scientific Research from the Ministry of Education, Culture, Sports, Science and Technology. We thank Prof. Yasuhiro Mazaki (Kitasato University), Prof. Tohru Nishinaga (Tokyo Metropolitan University), and Dr. Yoshiyuki Kuwatani (VSN Inc.) for helpful discussions, Prof. Gaku Yamamoto (Kitasato University) for the lineshape analysis, and Prof. Fujiko Iwasaki (the University of Electro-Communications) for the X-ray analyses. Theoretical calculations were partly performed at the Research Center for Computational Science, Okazaki, Japan.

Supporting Information

Figures of ^{1}H and ^{13}C NMR, MS, and UV spectra of **1a–1c** and **3**, cyclic voltammograms of **1a–1c** and **3**, electronic absorption spectra of oxidized **1a** and **3**, and Cartesian coordinates of **1a**, **1a^{2+}**, and **1a^{4+}** and the molecular orbital phase and energy diagram for them. This material is available free of charge via the Internet at http://www.csj.jp/journals/bcsj/.

References

1 a) *TTF Chemistry: Fundamentals and Applications of Tetrathiafulvalene*, ed. by J.-i. Yamada, T. Sugimoto, Kodansha Springer, Berlin, **2004**. b) Special issue on molecular conductors ed. by P. Batail: *Chem. Rev.* **2004**, *104*, Issue 11.

2 a) G. Saito, Y. Yoshida, *Bull. Chem. Soc. Jpn.* **2007**, *80*, 1. b) J. M. Williams, J. R. Ferraro, R. J. Thorn, K. D. Carlson, U. Geiser, H. H. Wang, A. M. Kini, M. H. Whangbo, *Organic Superconductors (Including Fullerenes)*, Prentice Hall, Englewood Cliffs, NJ, **1992**.

3 a) M. Iyoda, M. Hasegawa, Y. Miyake, *Chem. Rev.* **2004**, *104*, 5085. b) J. O. Jeppesen, M. B. Nielsen, J. Becher, *Chem. Rev.* **2004**, *104*, 5115. c) J. L. Segura, N. Martín, *Angew. Chem., Int. Ed.* **2001**, *40*, 1372. d) M. R. Bryce, *J. Mater. Chem.* **2000**, *10*, 589. e) M. B. Nielsen, C. Lomholt, J. Becher, *Chem. Soc. Rev.* **2000**, *29*, 153. f) T. Jørgensen, T. K. Hansen, J. Becher, *Chem. Soc. Rev.* **1994**, *23*, 41.

4 a) M. Hasegawa, M. Iyoda, *Chem. Soc. Rev.* **2010**, *39*, 2420. b) D. B. Amabilino, J. Puigmartí-Luis, *Soft Matter* **2010**, *6*, 1605. c) D. Canevet, M. Sallé, G. Zhang, D. Zhu, *Chem. Commun.* **2009**, 2245. d) M. Iyoda, T. Nishinaga, M. Takase, *Heterocyclic Supramolecules II* in *Topics in Heterocyclic Chemistry*, ed. by K. Matsumoto, N. Hayashi, Springer-Verlag, Berlin, **2009**, Vol. 18, pp. 103–118. doi:10.1007/7081_2008_16. e) M. Iyoda, M. Hasegawa, H. Enozawa, *Chem. Lett.* **2007**, *36*, 1402.

5 a) M. Jørgensen, K. Bechgaard, T. Bjørnholm, P. Sommer-Larsen, L. G. Hansen, K. Schaumburg, *J. Org. Chem.* **1994**, *59*, 5877. b) J. Puigmartí-Luis, V. Laukhin, Á. P. del Pino, J. Vidal-Gancedo, C. Rovira, E. Laukhina, D. B. Amabilino, *Angew. Chem., Int. Ed.* **2007**, *46*, 238. c) T. Akutagawa, K. Kakiuchi, T. Hasegawa, S. Noro, T. Nakamura, H. Hasegawa, S. Mashiko, J. Becher, *Angew. Chem., Int. Ed.* **2005**, *44*, 7283. d) T. Kitahara, M. Shirakawa, S. Kawano, U. Beginn, N. Fujita, S. Shinkai, *J. Am. Chem. Soc.* **2005**, *127*, 14980. e) C. Wang, D. Zhang, D. Zhu, *J. Am. Chem. Soc.* **2005**, *127*, 16372.

6 a) S. Ahn, Y. Kim, S. Beak, S. Ishimoto, H. Enozawa, E. Isomura, M. Hasegawa, M. Iyoda, Y. Park, *J. Mater. Chem.* **2010**, *20*, 10817. b) Y. Honna, E. Isomura, H. Enozawa, M. Hasegawa, M. Takase, T. Nishinaga, M. Iyoda, *Tetrahedron Lett.* **2010**, *51*, 679. c) H. Enozawa, Y. Honna, M. Iyoda, *Chem. Lett.* **2007**, *36*, 1434. d) Y. Kobayashi, M. Hasegawa, H. Enozawa, M. Iyoda,

Chem. Lett. **2007**, *36*, 720.

7 a) H. Enozawa, M. Hasegawa, D. Takamatsu, K. Fukui, M. Iyoda, *Org. Lett.* **2006**, *8*, 1917. b) M. Hasegawa, H. Enozawa, Y. Kawabata, M. Iyoda, *J. Am. Chem. Soc.* **2007**, *129*, 3072. c) M. Hasegawa, H. Enozawa, M. Iyoda, *J. Synth. Org. Chem., Jpn.* **2008**, *66*, 1211. d) H. Enozawa, M. Hasegawa, E. Isomura, T. Nishinaga, T. Kato, M. Yamato, T. Kimura, M. Iyoda, *ChemPhysChem* **2009**, *10*, 2607. e) M. Hasegawa, Y. Kobayashi, K. Hara, H. Enozawa, M. Iyoda, *Heterocycles* **2009**, *77*, 837. f) K. Hara, M. Hasegawa, Y. Kuwatani, H. Enozawa, M. Iyoda, *Heterocycles* **2010**, *80*, 909. g) E. Isomura, T. Nishinaga, M. Iyoda, *Supramol. Chem.* **2011**, *23*, 304.

8 J. Hankache, O. S. Wenger, *Chem. Rev.* **2011**, *111*, 5138.

9 a) V. Khodorkovsky, L. Shapiro, P. Krief, A. Shames, G. Mabon, A. Gorgues, M. Giffard, *Chem. Commun.* **2001**, 2736. b) K. Lahlil, A. Moradpour, C. Bowlas, F. Menou, P. Cassoux, J. Bonvoisin, J.-P. Launay, G. Dive, D. Dehareng, *J. Am. Chem. Soc.* **1995**, *117*, 9995. c) S. V. Rosokha, J. K. Kochi, *J. Am. Chem. Soc.* **2007**, *129*, 828. d) M. Hasegawa, J.-i. Takano, H. Enozawa, Y. Kuwatani, M. Iyoda, *Tetrahedron Lett.* **2004**, *45*, 4109.

10 a) J. M. Spruell, A. Coskun, D. C. Friedman, R. S. Forgan, A. A. Sarjeant, A. Trabolsi, A. C. Fahrenbach, G. Barin, W. F. Paxton, S. K. Dey, M. A. Olson, D. Benítez, E. Tkatchouk, M. T. Colvin, R. Carmielli, S. T. Caldwell, G. M. Rosair, S. G. Hewage, F. Duclairoir, J. L. Seymour, A. M. Z. Slawin, W. A. Goddard, III, M. R. Wasielewski, G. Cooke, J. F. Stoddart, *Nat. Chem.* **2010**, *2*, 870. b) T. Yasuda, K. Tanabe, T. Tsuji, K. K. Coti, I. Aprahamian, J. F. Stoddart, T. Kato, *Chem. Commun.* **2010**, *46*, 1224. c) M. Yoshizawa, K. Kumazawa, M. Fujita, *J. Am. Chem. Soc.* **2005**, *127*, 13456.

11 a) J. B. Torrance, B. A. Scott, B. Welber, F. B. Kaufman, P. E. Seiden, *Phys. Rev. B* **1979**, *19*, 730. b) M. E. Kozlov, Y. Tanaka, M. Tokumoto, T. Tani, *Synth. Met.* **1995**, *70*, 987.

12 a) K.-i. Nakamura, T. Takashima, T. Shirahata, S. Hino, M. Hasegawa, Y. Mazaki, Y. Misaki, *Org. Lett.* **2011**, *13*, 3122. b) M. Iyoda, K. Hara, Y. Kuwatani, S. Nagase, *Org. Lett.* **2000**, *2*, 2217. c) H. Spanggaard, J. Prehn, M. B. Nielsen, E. Levillain, M. Allain, J. Becher, *J. Am. Chem. Soc.* **2000**, *122*, 9486. d) J. Lyskawa, M. Sallé, J.-Y. Balandier, F. Le Derf, E. Levillain, M. Allain, P. Viel, S. Palacin, *Chem. Commun.* **2006**, 2233.

13 A. Y. Ziganshina, Y. H. Ko, W. S. Jeon, K. Kim, *Chem. Commun.* **2004**, 806.

14 a) U. Kux, M. Iyoda, *Chem. Lett.* **1994**, 2327. b) M. Iyoda, M. Hasegawa, Y. Kuwatani, H. Nishikawa, K. Fukami, S. Nagase, G. Yamamoto, *Chem. Lett.* **2001**, 1146.

15 a) M. Iyoda, Y. Kuwatani, N. Ueno, M. Oda, *J. Chem. Soc., Chem. Commun.* **1992**, 158. b) M. Iyoda, *Adv. Synth. Catal.* **2009**, *351*, 984.

16 The activation free-energy ($\Delta G^{\neq}$) from *anti* to *syn* of **1a** is estimated as 11 kcal mol^{-1} by lineshape analysis at $-75\,°C$.

17 a) H. O. House, D. G. Koepsell, W. J. Campbell, *J. Org. Chem.* **1972**, *37*, 1003. b) M. Iyoda, T. Okabe, M. Katada, Y. Kuwatani, *J. Organomet. Chem.* **1998**, *569*, 225. c) M. Iyoda, T. Kondo, K. Nakao, K. Hara, Y. Kuwatani, M. Yoshida, H. Matsuyama, *Org. Lett.* **2000**, *2*, 2081.

18 The first oxidation potentials ($E^1_{1/2}$) of TTF and Ph-TTF are 0.36 and 0.38 V vs. SCE, respectively, and the conjugation with aryl moiety increases the $E^1_{1/2}$-value of TTF: see Ref. 15a.

19 Comproportionation constant (K_c) is defined as follow:

$$\mathbf{1} + \mathbf{1}^{2+} \overset{K_c}{\rightleftharpoons} 2(\mathbf{1}^{\bullet+})$$

The K_c value was calculated from the difference between the first ($E^1_{1/2}$) and the second ($E^2_{1/2}$) oxidation potentials. See also: C. Creutz, *Progress in Inorganic Chemistry: An Appreciation of Henry Taube*, ed. by S. L. Lippard, John Wiley & Sons, Inc., **1983**, Vol. 30, pp. 1–73. doi:10.1002/9780470166314.ch1.

20 The generation of cationic species using the successive addition of preliminary titrated $Fe(ClO_4)_3$ in CH_2Cl_2–MeCN (1:1) was evaluated by appearance and disappearance of the isosbestic point during the oxidation (See Figure S2).

21 Recent examples for electrochromism based on TTF oligomers. see: a) M. Iyoda, H. Enozawa, Y. Miyake, *Chem. Lett.* **2004**, *33*, 1098. b) K. Hara, M. Hasegawa, Y. Kuwatani, H. Enozawa, M. Iyoda, *Chem. Commun.* **2004**, 2042.

22 a) S. Hünig, G. Kießlich, H. Quast, D. Scheutzow, *Justus Liebigs Ann. Chem.* **1973**, 310. b) G. Schukat, E. Fanghänel, *J. Prakt. Chem.* **1985**, *327*, 767.

23 M. J. Frisch, G. W. Trucks, H. B. Schlegel, G. E. Scuseria, M. A. Robb, J. R. Cheeseman, G. Scalmani, V. Barone, B. Mennucci, G. A. Petersson, H. Nakatsuji, M. Caricato, X. Li, H. P. Hratchian, A. F. Izmaylov, J. Bloino, G. Zheng, J. L. Sonnenberg, M. Hada, M. Ehara, K. Toyota, R. Fukuda, J. Hasegawa, M. Ishida, T. Nakajima, Y. Honda, O. Kitao, H. Nakai, T. Vreven, J. A. Montgomery, Jr., J. E. Peralta, F. Ogliaro, M. Bearpark, J. J. Heyd, E. Brothers, K. N. Kudin, V. N. Staroverov, R. Kobayashi, J. Normand, K. Raghavachari, A. Rendell, J. C. Burant, S. S. Iyengar, J. Tomasi, M. Cossi, N. Rega, J. M. Millam, M. Klene, J. E. Knox, J. B. Cross, V. Bakken, C. Adamo, J. Jaramillo, R. Gomperts, R. E. Stratmann, O. Yazyev, A. J. Austin, R. Cammi, C. Pomelli, J. W. Ochterski, R. L. Martin, K. Morokuma, V. G. Zakrzewski, G. A. Voth, P. Salvador, J. J. Dannenberg, S. Dapprich, A. D. Daniels, Ö. Farkas, J. B. Foresman, J. V. Ortiz, J. Cioslowski, D. J. Fox, *Gaussian 09 (Revision B.01)*, Gaussian, Inc., Wallingford CT, USA, **2009**.

24 Recent studies of π-dimer of $TTF^{\bullet+}$: a) M.-B. S. Kirketerp, L. A. E. Leal, D. Varsano, A. Rubio, T. J. D. Jørgensen, K. Kilså, M. B. Nielsen, S. B. Nielsen, *Chem. Commun.* **2011**, *47*, 6900. b) M. D. Halling, J. D. Bell, R. J. Pugmire, D. M. Grant, J. S. Miller, *J. Phys. Chem. A* **2010**, *114*, 6622. c) I. G. Yoldi, J. S. Miller, J. J. Novoa, *Theor. Chem. Acc.* **2009**, *123*, 137.

25 P. R. Ashton, V. Balzani, J. Becher, A. Credi, M. C. T. Fyfe, G. Mattersteig, S. Menzer, M. B. Nielsen, F. M. Raymo, J. F. Stoddart, M. Venturi, D. J. Williams, *J. Am. Chem. Soc.* **1999**, *121*, 3951.

26 The geometry optimizations of cation radicals at the Hartree–Fock level with the 6-31G(d) basis set offered reasonable structures of EDT-TTF moiety with good reproducibility, whereas the DFT method gave only poor structures at EDT-TTF moieties. Similar results were found in the literature. See: E. Demiralp, W. A. Goddard, III, *J. Phys. Chem.* **1994**, *98*, 9781, and Ref. 9a.

27 See Supporting Information.

28 The spin contents of cation radicals were evaluated through double integration of the ESR spectra and comparison with 2,2,6,6-tetramethyl-1-piperidine-*N*-oxyl (TEMPO) radical and Mn marker under identical conditions.

29 For recent examples, see: a) F. Schödel, U. Tutsch, F. Isselbächer, D. Schweitzer, I. Sänger, M. Bolte, J. W. Bats, J. Müller, M. Lang, M. Wagner, H.-W. Lerner, *Eur. J. Inorg. Chem.* **2011**, 1205. b) J. Müller, J. Brandenburg, J. A. Schlueter, *Phys. Rev. B* **2009**, *79*, 214521. c) S. Yamashita, Y. Nakazawa, M. Oguni, Y. Oshima, H. Nojiri, Y. Shimizu, K. Miyagawa, K. Kanoda, *Nat. Phys.* **2008**, *4*, 459.

30 SIR92: A. Altomare, G. Cascarano, C. Giacovazzo, A. Guagliardi, M. C. Burla, G. Polidori, M. Camalli, *J. Appl. Crystallogr.* **1994**, *27*, 435.